Metallic Nanoparticles Self-sintering Using Microheater under Millisecond Pulse Heating

Wei, Lai; Dorrestein, Sander; van Zeijl, Henk; Zhang, Guoqi

DOI
10.1109/EuroSimE65125.2025.11006534

Publication date
2025

Document Version
Final published version

Published in
Proceedings - 2025 26th International Conference on Thermal, Mechanical and Multi-Physics Simulation and Experiments in Microelectronics and Microsystems, EuroSimE 2025

2025 26th International Conference on Thermal, Mechanical and Multi-Physics Simulation and Experiments in Microelectronics and Microsystems (EuroSimE) | 979-8-3503-9300-2/25/$31.00 ©2025 IEEE | DOI: 10.1109/EUROSIME65125.2025.11006534

Metallic Nanoparticles Self-sintering Using Microheater under Millisecond Pulse Heating

1st Lai Wei
Department of Microelectronics
Delft University of Technology
Delft, The Netherlands
lwei4@tudelft.nl

2nd Sander Dorrestein
Chip Integration Technology Center
Nijmegen,The Netherlands
sander.dorrestein@citc.org

3rd Henk van Zeijl
Department of Microelectronics
Delft University of Technology
Delft, The Netherlands
h.w.vanzeijl@tudelft.nl

4th Guoqi Zhang
Department of Microelectronics
Delft University of Technology
Delft, The Netherlands
g.q.zhang@tudelft.nl

***Abstract*—This study presents a novel approach for localized silver (Ag) nanoparticles (NPs) sintering using microheater arrays embedded within the Si substrate. By applying controlled pulse currents, these microheaters generate targeted heat pulses, enabling rapid and localized sintering while maintaining the surrounding device components at room temperature. This localized heating minimizes thermal stress caused by thermal expansion mismatches, as sintering completes within milliseconds. Compared to conventional sintering techniques, this method improves process efficiency, reduces power consumption, and provides precise spatial control over the sintered regions. The proposed approach offers a promising alternative for microelectronics packaging and integration, particularly in applications requiring precise thermal management.**

***Index Terms*—Metallic nanopartiles, Microheater, Sintering, Pulse heating, Packaging.**

I. Introduction

Sintering is a widely used process in materials science for consolidating powders into solid structures through heat or pressure without reaching the material's melting point [1]. It is essential in the production of ceramics, metals, and composites, playing a crucial role in applications such as electronic packaging [2] [3] [4] [5], additive manufacturing [6] [7] [8], and structural components. Traditional sintering techniques, such as pressure-assisted sintering [9] [10] and Solid-State Sintering [11], require exposing the entire device to elevated temperatures, which can lead to thermal stress and degradation of temperature-sensitive components. In electronic packaging, sintering is used to form conductive interconnects, particularly with nano-silver particles due to their high electrical and thermal conductivity. However, conventional sintering methods may require prolonged heating, which can induce defects and warping in multilayer structures. To address these limitations, alternative approaches such as Selective Laser Sintering (SLS) [12] have been developed, where a high-energy laser fuses specific regions of a powder bed to form solid layers. Despite its precision, SLS suffers from slow processing speed and high power consumption.

Microheaters offer a promising solution for localized sintering, as they provide precise and controlled heating while minimizing thermal impact on surrounding areas. These devices have been used in various applications, including microfluidics [13], gas sensing [14], and thermal therapy. In microelectronics, microheater arrays can be embedded in substrates to facilitate localized sintering of conductive materials, reducing energy consumption and processing time while preventing damage to heat-sensitive components [15]. Fig. 1 shows an example of a specific application of the microheater. S-shaped microheater arrays are fabricated and embedded on the substrate, where the interconnect holes are placed in the curved area of the microheater. Chip 1 and chip 2 are supposed to flip-chip packaged on both sides of the substrate. As in the conventional sintering process, the entire device needs to be heated to the same temperature. While in this study, the microheater arrays achieve a localized sintering. By this way, the use of microheater arrays can complete the sintering process in certain areas while keeping the rest device at room temperature, which should be a more time-saving and energy-efficient way in the chip packaging process.

This work presents a novel approach using microheater arrays for localized nanoparticles (NPs) sintering in electronic packaging. By applying controlled current pulses, these microheaters generate targeted heat at the sintering site, ensuring a rapid and efficient bonding process while maintaining the overall device temperature. To evaluate this method, Finite Element Method (FEM) simulations are employed by using Multiphysics Simulation Software COMSOL to study heat transfer and electrical behavior. The study explores how variations in pulse amplitude and duration influence sintering efficiency, aiming to optimize the process to improve reliability and energy efficiency in advanced microelectronics manufacturing.

979-8-3503-9300-2/25/$31.00 ©2025 IEEE Presented at the EuroSimE 2025 Conference

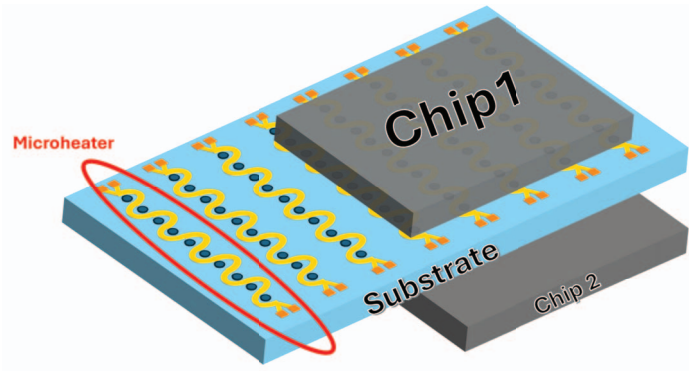

Fig. 1. Microheater arrays for sintering of flip-chip packaging.

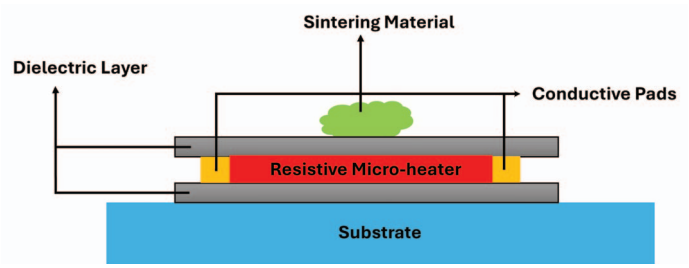

Fig. 2. Profile of microheater on substrate.

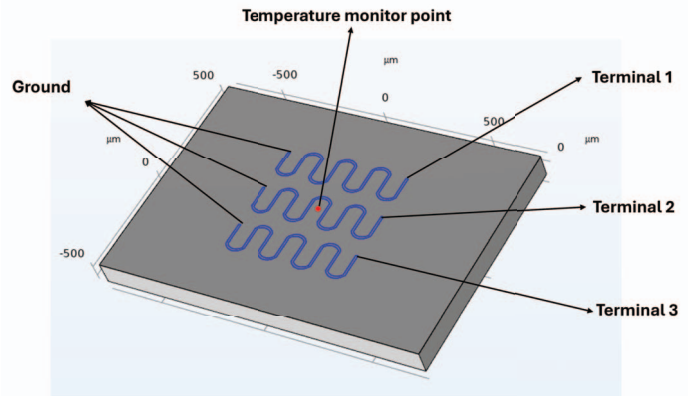

Fig. 3. Geometry model of microheater arrays.

II. Simulation

A. Design of microheater

In this study, the substrate is a block of $1500\,\mu\text{m} \times 1000\,\mu\text{m}$ with the thickness of $100\,\mu\text{m}$. The selection of the material for the substrate is crucial for the thermal performance of the microheater arrays. Si is a common material for the MEMS substrate and is compatible with most semiconductor fabrication conditions. However, in this simulation, glass is chosen as the substrate material for its its excellent properties such as optical transparency, electrical insulation, high thermal stability and low thermal expansion. A comparison of the properties of these two materials are shown in Table II-A. As shown in Fig. 3, three microheater arrays are placed parallel to each other on the substrate. The heating material should have a suitable electrical resistivity to generate heat efficiently when a voltage or current is applied. Depending on its size and application, a microheater typically functions at a kilohertz frequency, consuming approximately $100\,\text{mW}$ of power and reaching temperatures exceeding $1000\,^\circ\text{C}$. Common materials like Platinum (Pt), Nickel (Ni), Tungsten (W) are used for microheaters on different applications. Here, we use Titanium(Ti) as our heating material, the thickness of the microheater layer is $500\,\text{nm}$.

Fig. 2 shows the schematic diagram of the microheater, in which two dielectric layers are used for the electrical insulation of the resistive microheater. The metallic NPs paste is transferred on the top area of the top metal pad. Conductive pads will be used to apply the current pulse. To achieve a specific temperature, the time and current should be optimized depending on the sintering materials (Ag NPs, Cu NPs or others).

To simplify the model, the sintering material and interconnect inside the substrate are not included in this model as we will focus on the thermal properties of the microheater arrays.

B. Models and Methods

1) Geometry and Boundary Conditions:

- S-shaped microheater arrays were modeled as Ti thin films of $500\,\text{nm}$.
- The microheater arrays were embedded in a thin Si oxide layer of $1\,\mu\text{m}$, which is on the top of the substrate of $1500\,\mu\text{m} \times 1000\,\mu\text{m} \times 100\,\mu\text{m}$
- Current pulses ($34\,\text{mA}$-$40\,\text{mA}$) with certain periods were applied from Terminal 1,2 and 3 while the other ends of the arrays were grounded.
- The sides of the substrate and the oxide layer were modeled as open boundaries with a heat transfer coefficient of $h = 5\,\text{W/m}^2\times\text{K}$
- The initial temperature of the whole model is $20\,^\circ\text{C}$

2) Numerical Simulation Methods: The joule heating effect of the microheater arrays was modeled to investigate

TABLE I
Properties of Materials

Parameters	Materials		
	Titanium (20°C)	***Glass***	***Silicon***
Electrical Conductivity (S/m)	2.06×10^6	n/a	3100
Thermal Conductivity (W/(m · K))	21.9	1.16	111
Thermal Expansion Coefficient (W/(m · K))	8×10^{-6}	3.2×10^{-6}	2.6×10^{-6}
Young's Modulus (Pa)	1.61×10^{11}	7.29×10^{10}	1.7×10^{11}
Density ((kg/m^3))	4500	2230	2330
Heat Capacity (J/(kg · K))	504	703	681

its thermal performance. An electric current interface, which models input current pulses, was applied to perform the Joule heating effect in the numerical simulation. The main governing equations are the following:

$$\begin{aligned} \nabla \cdot J &= Q_j \\ J &= \sigma E + J_e \\ E &= -\nabla V \end{aligned} \tag{1}$$

where J is the current density $(\mathrm{A/m^2})$, Q_j is the external current source $(\mathrm{A/m^3})$, σ is electrical conductivity $(\mathrm{S/m})$, E is the electric field $(\mathrm{V/m})$, J_e is the external current density $(\mathrm{A/m^2})$, V is the electric potential (V). The electrical conductivity is a temperature-dependent variable, which is defined by (2).

$$\sigma = \frac{1}{\rho_0 \left(1 + \alpha \left(T - T_{ref}\right)\right)} \tag{2}$$

Where ρ_0 is the resistivity $(\Omega \cdot \mathrm{m})$, T_{ref} is the reference temperature of $20\,^{\circ}\mathrm{C}$ and α is the temperature coefficient of resistance $(1/\mathrm{K})$.

The heat transfer in solid interface was used to simulate the heat propagation in solid domains. The following equations were used as mathematical models to calculate this effect:

$$\begin{aligned} &\rho C_p \frac{\partial T}{\partial t} + \rho C_p \mathbf{u} \cdot \nabla T + \nabla \cdot \mathbf{q} = Q + Q_{\text{ted}} \\ &\mathbf{q} = -k \nabla T \end{aligned} \tag{3}$$

where ρ is the density of the material $(\mathrm{kg/m^{-3}})$, C_p $(\mathrm{J/(kg \cdot K)})$ is the solid heat capacity at constant pressure, $\vec{u}$ (m/s) is the velocity vector, $\vec{q}\,\mathrm{W/m^2}$ is the heat flux vector by conduction, k is the thermal conductivity (a scalar or a tensor if the thermal conductivity is anisotropic), Q $(\mathrm{W/m^3})$ the heat source (or sink), Q_{ted} represents the thermoelastic damping, which accounts for the thermoelastic effects in solids.

To get the current pulse inputted to the microheater arrays, an event interface was applied to control the ONOFF of the current, in which the period of the pulse current can be easily adjusted by the input time.

The whole model was calculated by a time-dependent solver with parameters sweep for the amplitude from $34\,\mathrm{mA}$ to $42\,\mathrm{mA}$ and the frequency from $50\,\mathrm{Hz}$ to $80\,\mathrm{Hz}$ of the current pulse. The variation of the frequency (f_p) corresponds to the change of pulse period (T_p) as they have the following relationship.

$$T_p = \frac{1}{f_p} \tag{4}$$

The total study time is $40\,\mathrm{ms}$, and the thermal performance of a single microheater and microheater arrays were investigated within this time.

Fig. 4 is a profile of the inputting current pulse within $40\,\mathrm{ms}$, with an amplitude of $0.038\,\mathrm{A}$ and a frequency of $80\,\mathrm{Hz}$ (corresponds to the period of $12.5\,\mathrm{ms}$).

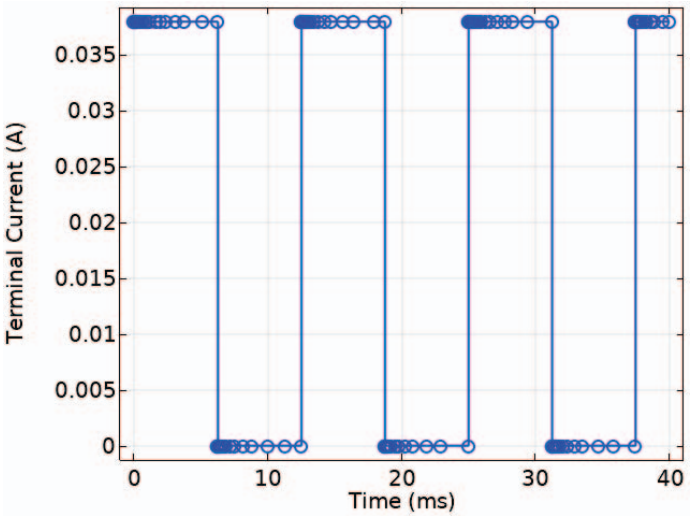

Fig. 4. Inputting current pulse.

III. Simulation Results

The following results present the temperature distribution and temperature change over time of the model, then the microheater's thermal performance is analysed and discussed.

A. Thermal Performance of A Single Microheater

1) Temperature distribution: 3D temperature distribution (with the amplitude of the current pulse of $0.04\,\mathrm{A}$ and a period of $\frac{1}{70}\mathrm{ms}$ at time equal to $35.732\,\mathrm{ms}$) on the surface of the model of a single microheater is shown in Fig. 5(a). The highest temperature occurs in the area around the microheater, while most of the rest area is kept below $100\,^{\circ}\mathrm{C}$. This shows a great localized heating performance of the microheater. To get a more detailed visualization of the temperature distribution around the microheater, 1D temperature distribution along the dashed line shown in Fig. 5(a) was outlined in Fig. 5(b), where the temperature gave a wave distribution as the microheater was in the heating period at this time. The peak of the temperature is where the microheater is located, and the valley should be where the sintering material would be added. More attention should be paid to the temperature of the sintering area, as the temperature related to the speed of the sintering process. As shown in Fig. 5, the temperature decreases significantly away from the microheater, so a potential way to speed up the sintering process could be a smaller and denser microheater's design.

Fig. 6 illustrates the 1D temperature distribution and variation over a period, a period consists of a heating cycle and cooling cycle. For example, the temperature distribution of time at $29\,\mathrm{ms}$, $32\,\mathrm{ms}$ and $35\,\mathrm{ms}$ correspond to the heating cycle in this period, while the time at $36\,\mathrm{ms}$ and $38\,\mathrm{ms}$ correspond to the cooling cycle. It can be concluded that the sintering area needs some time (several ms) to heat up after the start of the heating period of the microheater. Moreover, at the cooling period, the temperature of the sintering area would remain for about $1\,\mathrm{ms}$ when the microheater cooling down,

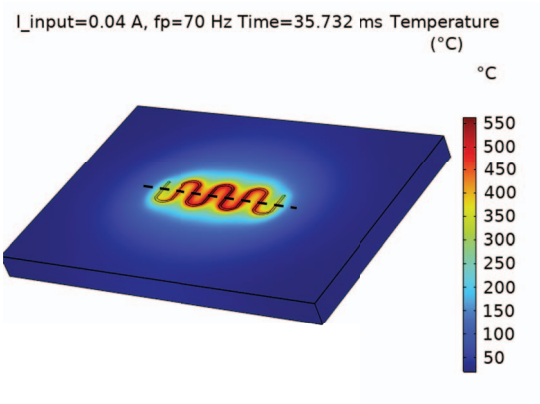

(a) 3D temperature distribution

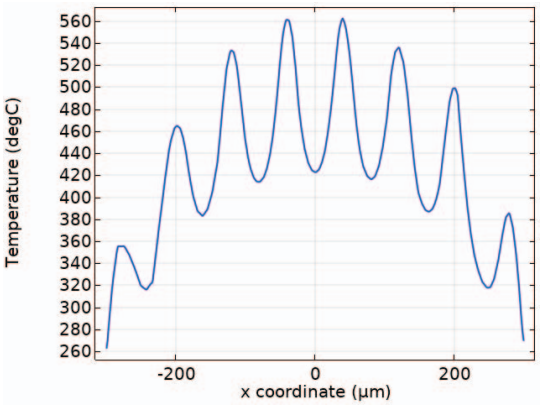

(b) 1D temperature distribution along the dashed line

Fig. 5. Temperature distribution of 3D and 1D

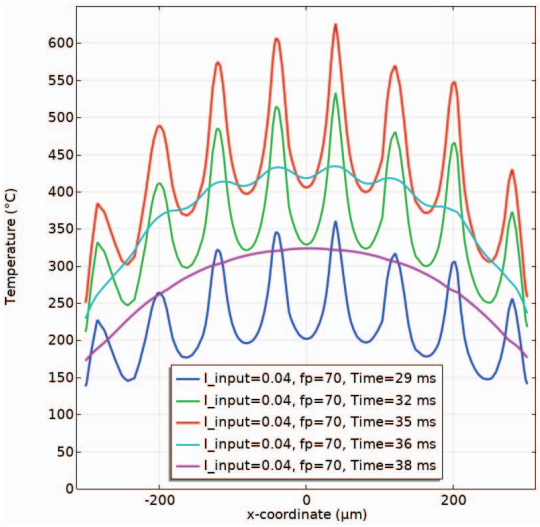

Fig. 6. 1D temperature distribution within 1 period.

this time should be the time needed for the heat dispersed to the sintering area.

2) Temperature variation over time: As mentioned above, the sintering area should be focused on as it will define the quality and speed of the sintering process. To get a visual understanding of the temperature variation over time, the temperature change at the red point of Fig. 3 was monitored over the whole study time. Fig. 7 shows the temperature change over time with different amplitudes and periods of the input current pulse.

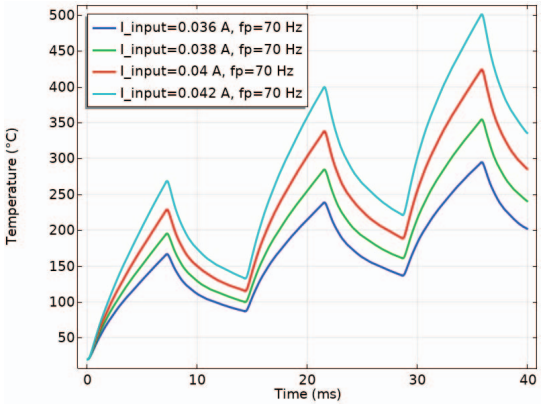

(a) Temperature variation over time with different amplitude of input current pulse

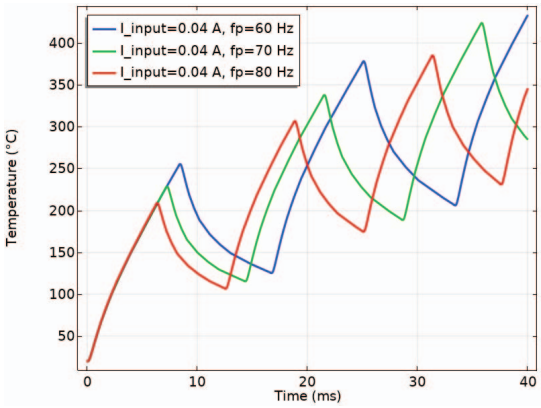

(b) Temperature variation over time with different period of input current pulse

Fig. 7. Temperature variation monitoring

It can be concluded from Fig. 7 that the temperature can be easily adjusted within the whole period by changing the amplitude and period of the input current pulse. To get a high temperature at the sintering area, one can easily do this by adding the amplitude of the current pulse or extending the heating cycle.

B. Thermal Performance of Microheater arrays

Fig. 8 and Fig. 9 show the thermal performance of microheater arrays. Fig. 8 is the temperature distribution of the 3 microheater arrays with the same period (at the heating cycle). Compared with a single microheater (shown in Fig. 5(a)), the microheater arrays has a better heating performance

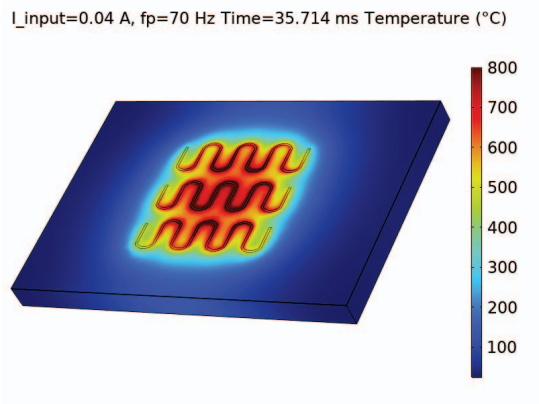

Fig. 8. Temperature distribution of microheater arrays with same period

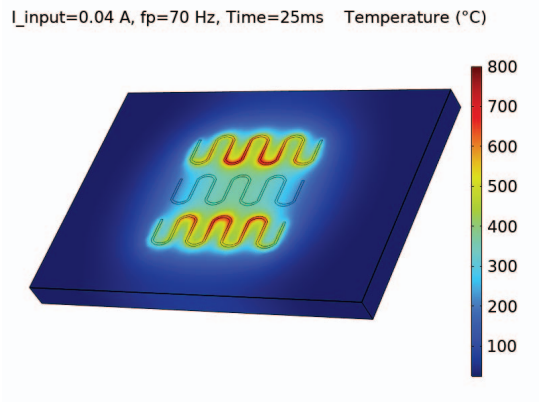

(a) Microheater 1 and 3 at the heating cycle while microheater 2 is in the cooling cycle

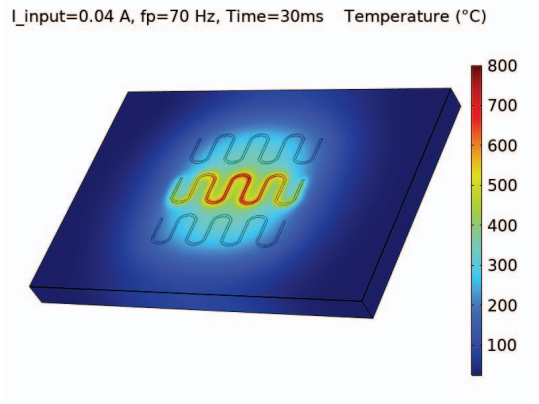

(b) Microheater 2 at the heating cycle while microheater 1 and 3 is in the cooling cycle

Fig. 9. Temperature distribution of microheater arrays with different periods

with a maximum temperature of $800\,^{\circ}\mathrm{C}$. Fig. 9 shows that the 3 microheater arrays can also work independently. The input current pulse of each microheater can be adjusted independently. Moreover, these results indicate that localized heating is effectively confined to the microheater region, which prevents heat-induced damage to surrounding components. Therefore, the design of the microheater arrays make the sintering process more localized and flexible.

As for the sintering process, there is a lot of research on pulsed light sintering, which can complete the sintering process within tens of milliseconds [16] [17] [18], Kang et al [18] have used 3 consecutive pulses at $50\,\mathrm{J/cm^2}$ to complete the nano-silver particles ($50\,\mathrm{nm}$) sintering in less than $30\,\mathrm{ms}$ by keeping the temperature at about $500\,^{\circ}\mathrm{C}$. Based on the simulation present in this work, the design of the microheater should be able to complete the nano-silver sintering within $40\,\mathrm{ms}$ as the highest local temperature can rise to around $700\,^{\circ}\mathrm{C}$, the experimental validation will be present in our future work.

IV. Conclusion

This paper presents the design and time-dependent simulation of the microheater arrays, the thermal performance was analysed according to the simulation results. By changing the amplitude and the period of the pulse current, the localized temperature can be easily changed. The use of microheater arrays also makes localized temperature control possible. These excellent thermal performances of the microheater arrays can be used for the nanoparticle sintering process. In conclusion, this makes the microheater arrays a promising method for the application of electronic device packaging.

Acknowledgment

The authors would like to acknowledge the financial support from the NXTGEN Hightech for the project Semcon 09 : NXTGEN Inlite (Inspiring Novel Light-Integrated Technology & Equipment).

References

[1] German, R.M., Suri, P. & Park, S.J. Review: liquid phase sintering. J Mater Sci 44, 1–39 (2009). https://doi.org/10.1007/s10853-008-3008-0

[2] Siow, K.S. Are Sintered Silver Joints Ready for Use as Interconnect Material in Microelectronic Packaging?. J. Electron. Mater. 43, 947–961 (2014). https://doi.org/10.1007/s11664-013-2967-3

[3] J. Fan, D. Xu, H. Zhang, C. Qian, X. Fan and G. Zhang, "Experimental Investigation on the Sintering Kinetics of Nanosilver Particles Used in High-Power Electronic Packaging," in IEEE Transactions on Components, Packaging and Manufacturing Technology, vol. 10, no. 7, pp. 1101-1109, July 2020.

[4] Yan, J. A Review of Sintering-Bonding Technology Using Ag Nanoparticles for Electronic Packaging. Nanomaterials 2021, 11, 927.

[5] G. -Q. Lu, W. Li, Y. Mei, G. Chen, X. Li and X. Chen, "Characterizations of Nanosilver Joints by Rapid Sintering at Low Temperature for Power Electronic Packaging," in IEEE Transactions on Device and Materials Reliability, vol. 14, no. 2, pp. 623-629, June 2014.

[6] Tuncer, N., Bose, A. Solid-State Metal Additive Manufacturing: A Review. JOM 72, 3090–3111 (2020). https://doi.org/10.1007/s11837-020-04260-y

[7] Seyed Farid Seyed Shirazi et al 2015 Sci. Technol. Adv. Mater. 16 033502

[8] Manfredi D, Ambrosio E P, Calignano F, et al. Direct metal laser sintering: an additive manufacturing technology ready to produce lightweight structural parts for robotic applications[J]. La metallurgia italiana, 2013.
[9] Antou, G., Guyot, P., Pradeilles, N. et al. Identification of densification mechanisms of pressure-assisted sintering: application to hot pressing and spark plasma sintering of alumina. J Mater Sci 50, 2327–2336 (2015).
[10] Branislav Dzepina, Daniel Balint, Daniele Dini, A phase field model of pressure-assisted sintering, Journal of the European Ceramic Society, Volume 39, Issues 2–3, 2019, Pages 173-182.
[11] Zheng, J., & Reed, J. S. (1989). Effects of particle packing characteristics on solid-state sintering. Journal of the American ceramic Society, 72(5), 810-817.
[12] Kruth, J. P., Wang, X., Laoui, T., & Froyen, L. (2003). Lasers and materials in selective laser sintering. Assembly Automation, 23(4), 357-371.
[13] Son, J. M., Lee, J. H., Kim, J., & Cho, Y. H. (2015). Temperature distribution measurement of Au microheater in microfluidic channel using IR microscope. International Journal of Precision Engineering and Manufacturing, 16, 367-372.
[14] Bhattacharyya, P. (2014). Technological journey towards reliable microheater development for MEMS gas sensors: A review. IEEE Transactions on device and materials reliability, 14(2), 589-599.
[15] Holt, N., & Zhou, W. (2018). Design and Fabrication of an Experimental Microheater Array Powder Sintering Printer. JOM, 70, 1785-1792.
[16] Peng, P., Hu, A. & Zhou, Y. Laser sintering of silver nanoparticle thin films: microstructure and optical properties. Appl. Phys. A 108, 685–691 (2012). https://doi.org/10.1007/s00339-012-6951-1
[17] Shankar, A., Salcedo, E., Berndt, A. et al. Pulsed light sintering of silver nanoparticles for large deformation of printed stretchable electronics. Adv Compos Hybrid Mater 1, 193–198 (2018). https://doi.org/10.1007/s42114-017-0012-3
[18] Kang, J.S., Ryu, J., Kim, H.S. et al. Sintering of Inkjet-Printed Silver Nanoparticles at Room Temperature Using Intense Pulsed Light. J. Electron. Mater. 40, 2268–2277 (2011). https://doi.org/10.1007/s11664-011-1711-0